Reviews in Mineralogy & Geochemistry
Vol. 71 pp. 465-484, 2010

Thermodynamics of the Earth's Mantle

Lars Stixrude and Carolina Lithgow-Bertelloni

Department of Earth Sciences
University College London
Gower Street
London WC1E 6BT, United Kingdom

l.stixrude@ucl.ac.uk

INTRODUCTION

Central to the goals of mineral physics is an elucidation of how material behavior governs planetary processes. Planetary accretion, differentiation into crust, mantle, and core, ongoing processing by magmatism, dynamics and thermal evolution, and the generation of magnetic fields, are all processes controlled by the physical properties and phase equilibria of planetary materials. Knowledge of these processes has advanced in large measure by progress in the study of material behavior at extreme conditions of pressure and temperature.

Thinking of a planet as an experimental sample emphasizes the relationship between planetary processes and material behavior via properties that control its response to natural perturbations. We may explore the response of the planet to a sudden increase in energy, provided, for example, by a giant impact of the type that is thought to have formed Earth's moon (Canup 2004). Responses include an increase in temperature, controlled by the heat capacity, a decrease in density controlled by the thermal expansivity, and phase transformations controlled by the free energy. Phase transformations also contribute to changes in temperature and density via the heats and volumes of transformation. A giant impact also perturbs the stress state, to which the planet responds via compression (controlled by the bulk modulus), adiabatic heating (Grüneisen parameter) and phase transformations (free energy).

A planet is an unusual experimental sample because its pressure is self-generated via gravitational self-compression, and its temperature via adiabatic compression and radioactive decay. Indeed one of the major challenges in understanding planetary-scale processes is that the characteristic pressure (1 Mbar) and temperature (several thousand K) are so large. Consider an Earth-like planet in which the mantle makes up 2/3 of the mass and the core makes up the remainder. The pressure P_M at the base of the mantle depends approximately linearly on planetary mass M: P_M(Mbar)~1.4(M/M_E), as does the temperature at the base of the mantle due to adiabatic compression T_M(K) ~1600+1000(M/M_E), assuming the potential temperature to be set by silicate melting, as it is on Earth (Valencia et al. 2006).

First principles theory of the kind discussed elsewhere in this volume has played a major role in the elucidation of planetary processes in large part because it is able to access with ease the extreme conditions of planetary pressure and temperature. Density functional theory in particular has had a tremendous impact because it is equally applicable to all conditions of planetary pressure and temperature and in principle to all elements of the periodic table (Kohn 1999), although some major elements are more problematic than others, such as Fe in oxides and silicates (Gramsch et al. 2003; Cococcioni 2010; Wentzcovitch et al. 2010). Methods with in-principle even greater scope and accuracy, including improved functionals and Quantum Monte Carlo, are being developed (Mitas and Kolorenč 2010; Perdew and Ruzsinszky 2010). By comparison, static experiments have only recently been able to access pressure-temperature

1529-6466/10/0071-0021$05.00 DOI: 10.2138/rmg.2010.71.21

conditions of Earths' core-mantle boundary routinely and to perform a variety of precise measurements *in situ* (Murakami et al. 2004, 2007; Mao et al. 2006). Continued advances in theory and experiment are both important because density functional theory is not exact and produces small, systematic errors that are well understood, but persistent, while experiments at extreme conditions can produce contradictory results because they are often pushing the envelope of what is technologically feasible.

As experimental samples, planetary mantles are unusual in at least one other respect that presents challenges to first principles theory and experiment: they are chemically complex and heterogeneous. In Earth's mantle there are at least 6 essential chemical components (SiO_2, MgO, FeO, CaO, Al_2O_3 Na_2O), that stabilize a large number of impure phases over the entire mantle pressure-temperature regime, and a host of minor elements that may also play an important role in planetary processes, such as H_2O and CO_2 (Hirschmann 2006; Ohtani and Sakai 2008). The length scale of heterogeneity is known to range from the grain scale represented by adjoining phases of contrasting physical properties, such as olivine and spinel in a typical xenolith, to that of lithologic banding, represented by pyroxenite veins in obducted peridotites, and may include much larger scales as well (Allegre and Turcotte 1986). Mantle convection appears not to be as efficient at homogenizing major element composition as had once been thought and may be compatible with planet-scale variations in bulk composition between upper and lower mantle, perhaps driven by lithologic density contrasts (Xie and Tackley 2004).

Understanding planetary processes then demands a method complementary to first principles calculations and experiment that is able to interpolate among and extrapolate from necessarily limited results to the full chemical richness that is typical of silicate mantles. Here we review a method, based on new developments in thermodynamic theory and a careful analysis of the information provided by experiment and first principles theory that permits the construction of realistic models of planetary interiors. This method allows one to fully capture the heterogeneity inherent in the relevant multi-component, multi-phase equilibria and the physical properties of the multi-phase assemblages. The method is complementary to first principles theory and experiment and indeed uses results on simple systems to build up predictive power for more complex and relevant assemblages. There have been many previous attempts to construct thermodynamic models of Earth's mantle. We show below that all of these have important limitations. We show how our method can be used to address mantle heterogeneity on all length scales ranging from that of the subducting slab to the possibility of mantle-wide radial variations in bulk composition.

OUR APPROACH AND PREVIOUS WORK

The key difference between our approach and previous models is our adherence to thermodynamic self-consistency (Stixrude and Lithgow-Bertelloni 2005b). This adherence has the important advantage that all thermodynamic relations including the Maxwell relations and the Clapeyron equation are uniquely satisfied. There are practical advantages as well: because so many thermodynamic quantities are intimately linked, diverse experimental and first principles results can be used independently to constrain more robustly the thermodynamic model. For example, phase equilibria and equation of state data both constrain the volume of a phase, placing redundant constraints on the equation of state. Another important difference is the scope of our model. Whereas many models of the mantle have been primarily focused on either phase equilibria, or physical properties, our approach is to self-consistently describe both, differing fundamentally from so-called hybrid models in which some sub-set of physical properties are computed self-consistently and phase equilibria are determined independently and non-self-consistently (Ita and Stixrude 1992; Cammarano et al. 2003; Hacker et al. 2003). The important point being that phase transformations influence physical properties as much as the effects of pressure and temperature on single phases over the mantle range, a feature that

our approach naturally encompasses.

Our approach makes use of four sets of thermodynamic principles that, except for the last, have featured in other contexts, but have not before been combined in application to Earth's mantle:

Fundamental thermodynamic relations

A fundamental thermodynamic relation is a single functional relationship that contains complete information of all equilbrium properties of all equilibrium states of a particular species (Callen 1960; Stixrude and Bukowinski 1990). All thermodynamic properties are computed as derivatives of the fundamental relation with respect to its natural variables, guaranteeing self-consistency. For example

$$\frac{\partial^3 G}{\partial P \partial P \partial T} = \frac{\partial^3 G}{\partial T \partial P \partial P} = \frac{\partial}{\partial P}\left(V\alpha\right)_T = \frac{\partial}{\partial T}\left(\frac{V}{K}\right)_P \tag{1}$$

where G is the Gibbs free energy, P is pressure, T is temperature, V is volume, α is thermal expansivity, and K is the isothermal bulk modulus. We write the fundamental relation in analytic form with analytically computable derivatives so that relations of this type are satisfied exactly. Some previous models of mantle thermodynamics violate the Maxwell relations (Sobolev and Babeyko 1994).

Euler form

In our model the fundamental thermodynamic relation is written in Euler form, which is always possible because of the first order homogeneity of thermodynamic functions. The importance of the Euler form, in which the thermodynamic potential appears as an absolute quantity, e.g., $G = G(P,T)$, is important for applications to planetary mantles and differs from the more common use of the differential form

$$dG = -SdT + VdP \tag{2}$$

which must be integrated to determine the value of G at the pressure and temperature of interest. The integration is typically performed along a path that proceeds in two legs: first upwards in temperature at ambient pressure and second upwards in pressure at elevated temperature (Berman 1988; Fei and Saxena 1990; Ghiorso and Sack 1995; Holland and Powell 1998). The advantage of the differential approach is that it maintains close contact with experimental measurements at ambient pressure of the volume and the entropy S (via integration of measurements of the heat capacity). The differential approach is adequate as long as the temperature and pressure are not too high, but has at least three difficulties in application to Earth's mantle:

1) The temperature in the middle of Earth's mantle is approximately 2000 K and may be 4000 K at its base. This temperature far exceeds melting points at ambient pressure. This means that the initial leg of the integration path must extend into the super-solidus regime where no thermodynamic data on the crystalline phase of interest exist and where the crystalline phase of interest may be mechanically unstable.

2) The term VdP dominates over most of Earth's mantle and must be treated with greater care than is possible using the differential form. For example, the change in Gibbs free energy along a mantle isotherm far exceeds the difference in Gibbs free energy between 300 K and 2000 K. Moreover, the increase in G along the isotherm quickly surpasses in magnitude even the Gibbs free energy of formation from the elements at depths as shallow as the transition zone.

3) Some mantle phases (e.g. post-perovskite) are unquenchable to ambient pressure, rendering the first leg of the integration path ill-defined.

Legendre transformations

While the Gibbs free energy is the natural thermodynamic potential for treating phase equilibria, the Helmholtz free energy is much more convenient for describing the equation of state. Legendre transformations provide a simple way of moving from one thermodynamic potential to the other (Alberty 2001). So for example, the Helmholtz free energy F is related to G by

$$G(P,T) = F(V,T) + PV(P,T) \tag{3}$$

We may then describe the variation of the Gibbs free energy with pressure in terms of the most successful account of the equation of state, which is formulated as the volume derivative of Helmholtz free energy (Birch 1978). This overcomes the poor convergence of equations of state based on power series expansions of G in P, or the Murnaghan equation, as used in many thermodynamic models popular in the Earth sciences (Ghiorso and Sack 1995; Holland and Powell 1998).

Anisotropic generalization

A final key feature of our model and a new theoretical development is the generalization of the thermodynamic machinery to the consideration of deviatoric stress and strain in such a way that fully self-consistent computation of phase equilibria and the elastic constant tensor is possible. This final step is essential for making contact with seismological observations and we are not aware of another thermodynamic model that has this capability. Previous mantle models have either not specified the shear modulus or other components of the elastic moduli (Mattern et al. 2005), or have done so non-self-consistently (Kuskov 1995; Hama and Suito 1998). Our derivation is given fully elsewhere (Stixrude and Lithgow-Bertelloni 2005b) and builds on previous work in relating thermodynamic potentials to elasticity (Wallace 1972; Davies 1974). The analysis is based on a polynomial expansion of the thermodynamic potential in the Eulerian finite strain with special attention paid to the distinction between the large finite strain associated with the Earth's internal pressure and the much smaller strain of general symmetry applied by a passing seismic wave.

THERMODYNAMIC THEORY

Our thermodynamic method has been derived elsewhere and our purpose here is to summarize the theory, sketch its derivation, and highlight some of its key features (Stixrude and Lithgow-Bertelloni 2005a,b).

The Gibbs free energy of the multi-phase assemblage

$$G(\sigma_{ij},T,n_\beta) = \sum_\beta n_\beta \mu_\beta(\sigma_{ij},T,n_\beta) = \sum_\beta n_\beta \left[G_\beta(\sigma_{ij},T) + RT \ln a_\beta \right] \tag{4}$$

where the sum is over all species (end-members) in the model n_β is the number of moles of species β, μ_β is the chemical potential, G_β is the Gibbs free energy of pure species β, R is the universal gas constant a_β is the activity, and the stress is related to pressure by

$$\sigma_{ij} = -P\delta_{ij} + \tau_{ij} \tag{5}$$

where τ_{ij} is the deviatoric stress. We assume that the quantity $RT\ln f_\beta$ is independent of pressure and temperature, where f_β is the activity coefficient that relates activity to concentration (Ita and Stixrude 1992). This assumption permits non-ideal enthalpy of solution, but neglects the contribution of non-ideailty to other physical properties, such as volume or entropy, because such contributions are small compared with uncertainties in these properties at mantle pressure and temperature. We also neglect surface energy, which may be significant for very small grains (~1 nm).

The Gibbs free energy of the pure species G_β is specified by the Legendre transformation of the Helmholtz free energy

$$F(E_{ij},T) = F_0(0,T_0) + F_c(E_{ij},T_0) + \Delta F_q(E_{ij},T) \tag{6}$$

where we have suppressed the index β, the first three terms on the right hand side are respectively the reference value at the natural configuration, and the contributions from compression at ambient temperature (the so-called "cold" part), and lattice vibrations in the quasi-harmonic approximation. These are expected to be the most important for the physical properties of mantle phases. Additional contributions to order-disorder transitions such as the α-β quartz transition (Landau term), and a magnetic term to account for spin disorder are discussed in a forthcoming publication and will not be further addressed here. The E_{ij} is the Eulerian finite strain relating the "natural" state at ambient conditions with material points located at coordinates a_i, to the "final" state with coordinates x_i. Thermodynamic quantities are related to the strain S_{ij} that relates the final state to the initial or pre-stressed state with coordinates X_i. We assume that the initial state is one of hydrostatic stress, appropriate to the earth's interior, and that the final state differs slightly from the initial state, corresponding to the small amplitude of seismic waves. We view the natural configuration as that at ambient pressure and temperature, corresponding to the "master" configuration of Davies (1974).

We have argued that the following form of the Helmholtz free energy is appropriate

$$\rho_0 F_c(E_{ij},T) = \frac{1}{2} b^{(1)}_{ijkl} E_{ij} E_{kl} - \frac{1}{6} b^{(2)}_{ijklmn} E_{ij} E_{kl} E_{mn} + \frac{1}{24} b^{(3)}_{ijklmnop} E_{ij} E_{kl} E_{mn} E_{op} + \ldots \tag{7}$$

$$\rho_0 F_q(E_{ij},T) = \rho_0 nRT \left[\frac{\theta(E_{ij})}{T}\right]^{-3} \int_0^{\theta(E_{ij})/T} \ln\left(1-e^{-t}\right) t^2 dt \tag{8}$$

where ρ is the density, n is the number of atoms in the formula unit, θ is the Debye temperature and subscript 0 indicates values at ambient conditions. We find the equation of state and isothermal elastic constants by taking the appropriate strain derivatives and evaluating in the initial state; correct to fourth order in the strain

$$\rho_0 F = \rho_0 F_0 + \frac{1}{2} b^{(1)}_{iikk} f^2 + \frac{1}{6} b^{(2)}_{iikkmm} f^3 + \frac{1}{24} b^{(3)}_{iikkmmoo} f^4 + \rho_0 \Delta F_q \tag{9}$$

$$P = \frac{1}{3}(1+2f)^{5/2}\left[b^{(1)}_{iikk} f + \frac{1}{2} b^{(2)}_{iikkmm} f^2 + \frac{1}{6} b^{(3)}_{iikkmmoo} f^3\right] + \gamma\rho\Delta U_q \tag{10}$$

$$\begin{aligned} c_{ijkl} = (1+2f)^{5/2} &\left\{ c_{ijkl0} + \left(3K_0 c'_{ijkl0} - 5c_{ijkl0}\right) f \right. \\ &\left. + \left[6K_0 c'_{ijkl0} - 14 c_{ijkl0} - \frac{3}{2} K_0 \delta^{ij}_{kl}\left(3K'_0 - 16\right)\right] f^2 \right\} \\ &+ \left[\gamma_{ij}\gamma_{kl} + \frac{1}{2}\left(\gamma_{ij}\delta_{kl} + \gamma_{kl}\delta_{ij}\right) - \eta_{ijkl}\right]\rho\Delta U_q - \gamma_{ij}\gamma_{kl}\rho\Delta\left(C_V T\right) \end{aligned} \tag{11}$$

where U is the internal energy, C_V is the isochoric heat capacity, c_{ijkl} is the elastic constant tensor, $\delta^{kl}_{ij} = -\delta_{ij}\delta_{kl} - \delta_{ik}\delta_{jl} - \delta_{il}\delta_{jk}$, the prime indicates pressure derivative and the parenthetical superscripts provide a convenient way of distinguishing among the coefficients when alternating between standard and Voigt notation (Davies 1974). We have assumed an isotropic state of initial finite strain

$$E_{ij} = -f\delta_{ij} \tag{12}$$

$$f = \frac{1}{2}\left[\left(\frac{\rho}{\rho_0}\right)^{2/3} - 1\right] \tag{13}$$

The Grüneisen parameter $\gamma = V(\partial P/\partial U)_V$, the Grüneisen tensor

$$\gamma_{ij} = -\frac{\partial \ln \theta}{\partial S_{ij}} \tag{14}$$

and $\gamma_{ii} = \gamma\delta_{ii}$ for an isotropic material. The adiabatic elastic moduli follow from $c_{ijkl}^S = c_{ijkl} - \gamma_{ij}\gamma_{kl}\rho C_V T$.

The isothermal bulk modulus and the shear modulus of an isotropic material follow from $3K = c_{ijkl}\delta_{ij}\delta_{kl}/3$ and $G = c_{44} = (c_{11} - c_{12})/2$

$$K = (1+2f)^{5/2}\left[K_0 + (3K_0K_0' - 5K_0)f + \frac{27}{2}(K_0K_0' - 4K_0)f^2\right] + (\gamma + 1 - q)\gamma\rho\Delta U_q - \gamma^2\rho\Delta(C_V T) \tag{15}$$

$$G = (1+2f)^{5/2}\left[G_0 + (3K_0G_0' - 5G_0)f + \left(6K_0G_0' - 24K_0 - 14G_0 + \frac{9}{2}K_0K_0'\right)f^2\right] - \eta_S\rho\Delta U_q \tag{16}$$

where $q = (\partial \ln\gamma/\partial \ln V)$, and η_S is the shear part of the tensor

$$\eta_{ijkl} = \frac{\partial \gamma_{ij}}{\partial S_{kl}} \tag{17}$$

which for an isotropic material is

$$\eta_{ijkl} = \gamma q \delta_{ij}\delta_{kl} + \eta_S\left(\delta_{ik}\delta_{jl} + \delta_{il}\delta_{jk} - \frac{2}{3}\delta_{ij}\delta_{kl}\right) \tag{18}$$

We assume that the strain dependence of the Debye temperature is expressed as a power series in the finite strain

$$\theta^2 = \theta_0^2\left[1 + 6\gamma_0 f + \frac{1}{2}(-12\gamma_0 + 36\gamma_0^2 - 18q_0\gamma_0)f^2 + \ldots\right] \tag{19}$$

which has been evaluated at the initial state.

We assume that the activity has two contributions, an ideal contribution, given by ideal mixing of unlike cations on multiple sites (Thompson 1969) and a non-ideal contribution given by the symmetric regular solution formulation. We assume that the excess Gibbs free energy is independent of pressure and temperature. This seems justified by the fact that excess volume and entropy are either unmeasured or small for most mantle phases. Moreover, when they can be measured precisely, as in the case of the excess volume, the measurements exist only at 1 bar and may not be representative of the excess volume at the pressure of interest, where it may even be of opposite sign.

Some of the scope and goals of the model are illustrated by an example (Fig. 1). We have computed the phase equilibria and physical properties of a typical mantle bulk composition (Workman and Hart 2005) along a self-consistently computed isentrope with a potential temperature of 1600 K, approximately that required by the generation of mid-ocean ridge basalt (McKenzie and Bickle 1988). The phase equilibria are consistent with experimental results

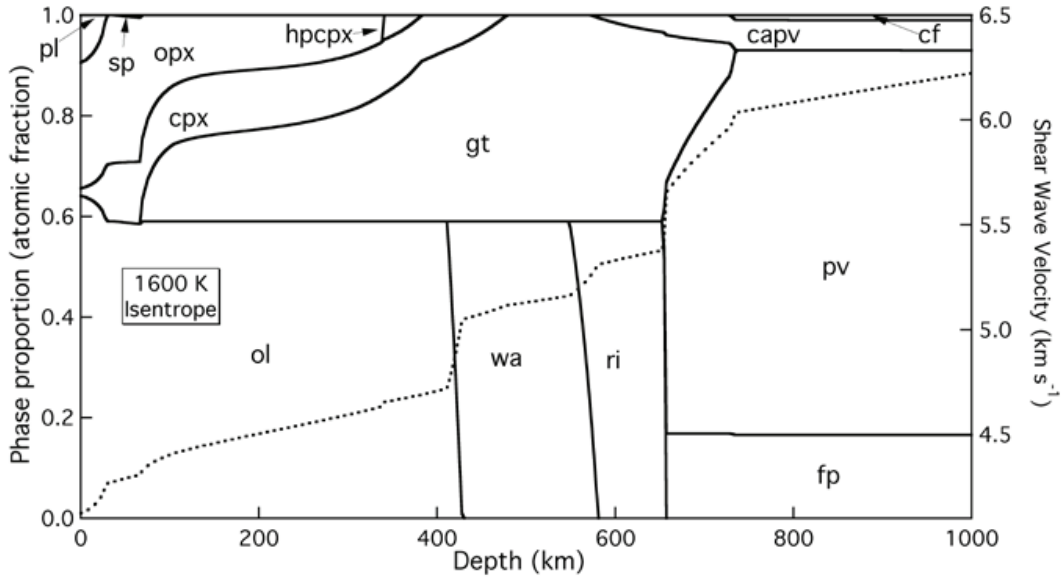

Figure 1. Computed phase equilibria (solid, left axis) and self-consistent shear wave velocity (dashed, right axis) along a self-consistently computed isentropic temperature profile assuming a potential temperature of 1600 K, according to our thermodynamic theory and our latest set of published parameters (Xu et al. 2008). Phases are: plagiolcase (plg), spinel (sp), olivine (ol), orthopyroxene (opx), clinopyroxene (cpx), high-pressure Mg-rich clinopyroxene (hpcpx), garnet (gt), wadsleyite (wa), ringwoodite (ri), akimotoite (ak), Calcium silicate perovskite (capv), Magnesium-rich silicate perovsite (pv), ferropericlase (fp), and Calcium-Ferrite structured phase (cf).

and with constraints imposed by xenoliths, including the transition from spinel-bearing to garnet-bearing assemblages, and the gradual dissolution of pyroxenes into garnet (Boyd 1989; Collerson et al. 2000). The computed shear wave velocity is also consistent with experimental results and bears many similarities to that seismologically observed in the mantle, in particular the locations of major "discontinuities" near 410 and 660 km depth, and the steeper velocity gradient in between these two boundaries (Dziewonski and Anderson 1981). The way in which such computations form a foundation from which the thermal and chemical state of Earth can be determined is illustrated further in the Applications section below.

CONSTRAINING AND TESTING THE MODEL

The thermodynamic theory contains a total of ten free parameters for each of the mantle species. These are F_0, V_0, K_0, K_0', G_0, G_0', θ_0, γ_0, q_0, η_{S0}, respectively the values at ambient conditions of the Helmholtz free energy, volume, bulk modulus and its pressure derivative, the shear modulus and its pressure derivative, the Debye temperature, its logarithmic volume derivative the Grüneisen parameter, and the logarithmic volume derivative of γ, and the second derivative of the Debye temperature with respect to shear strain. In addition the activities of mantle species in solution are specified by symmetric regular solution parameters $W_{\alpha\beta}$. These are defined only for those phases for which thermochemical data or phase equilibria data demand non-ideal contributions to the Gibbs free energy.

The values of the parameters are determined by comparing primarily with experimental data (Stixrude and Lithgow-Bertelloni 2005b; Xu et al. 2008). Sufficient experimental information now exists to constrain all the relevant parameters for at least the most abundant species of all relevant phases. In cases where no experimental data are available, we estimate the values of the parameters from systematic relationships, for example Birch's law (Anderson et al. 1968), or from the results of first principles theory.

First principles calculations are most powerful as a means of identifying functional relationships among thermodynamic quantities and testing the forms assumed in the construction of our thermodynamic theory. First principles calculations are able to sample much greater ranges of pressure and temperature and with much greater precision than experiment, making functional relationships clear. Density functional theory also yields predictions of key material properties that have not yet been measured, but because it is not exact, and because experimental progress is rapid, experimental values are preferred where these are available.

Three examples show the ability of first principles calculations to reveal and test functional relationships:

Elastic constants

The ability of the Eulerian finite strain expansion to capture the physics of high pressure elasticity is illustrated by a comparison of our formulation with first principles predictions of the elastic constants of $MgSiO_3$ perovskite (Fig. 2) (Karki et al. 1997). The Eulerian finite strain formulation (Eqns. 15,16) is able to represent first principles results accurately with only two parameters (moduli and their first pressure derivatives). In contrast, an alternative formulation, using the Lagrangian finite strain fails completely, as does a simple linear function of pressure.

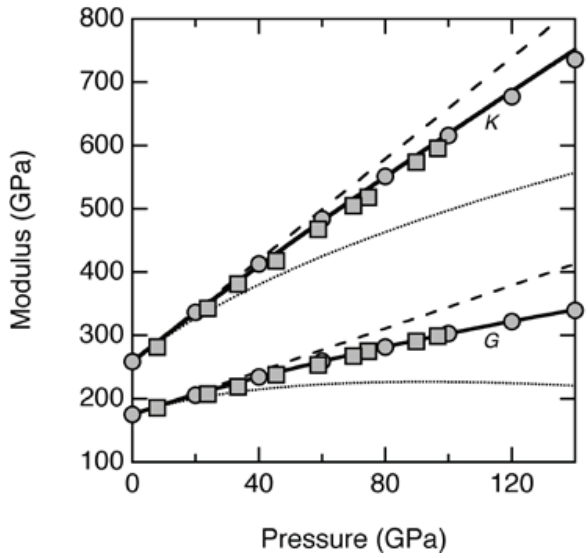

Figure 2. (solid lines) Eulerian third-order finite strain versus (short-dashed lines) Lagrangian third-order finite strain expressions and (long-dashed lines) a linear extrapolation compared with (circles) first principles results (Karki et al. 1997) and (squares) experimental results (Murakami et al. 2007) for the room temperature isothermal bulk modulus (K) and the shear modulus (G) of $MgSiO_3$ perovskite. For the purposes of this comparison, all curves were computed using values of $K_0 = 259$, $G_0 = 175$, $K_0' = 4.0$, and $G_0' = 1.7$ taken from the first principles study. (Modified from Stixrude and Lithgow-Bertelloni 2005b).

Grüneisen parameter and q

First principles predictions show that the volume dependence of the Grüneisen parameter differs significantly from the usual assumption of constant q. Instead, q itself is found to decrease substantially on compression (Karki et al. 2000a,b; Oganov et al. 2001a; Oganov and Dorogokupets 2003). These patterns are captured by our thermodynamic theory and indeed served as inspiration for choosing to describe the volume dependence of the vibrational frequency as a power series in finite strain (Eqn. 19) (Fig. 3). In fact previous results perhaps show a somewhat stronger volume dependence of q than predicted by third order Eulerian finite strain theory, although the scatter is substantial. The value of q at high pressure is important because it controls lateral variations with temperature of the bulk sound velocity (Isaak et al. 1992).

Temperature dependence of the shear modulus

First principles calculations show that the temperature derivative of the shear modulus depends strongly on compression (Oganov et al. 2001b; Wentzcovitch et al. 2004), while many non-self-consistent mineralogical models in the past have assumed that dG/dT is independent of pressure (Cammarano et al. 2003). The agreement between the first principles studies is remarkable because they are based on different approximations to the exchange-correlation functional, and different methods for computing high temperature properties (molecular dynamics vs. lattice dynamics). Our thermodynamic theory, in which the volume dependence of η_S is determined by Equations (14) and (17) and the primitive form of Equation (19), appears

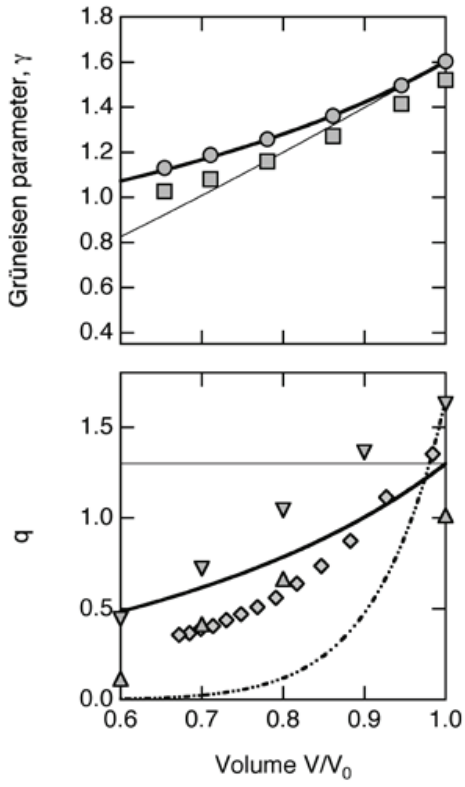

Figure 3. (top) Grüneisen parameter, γ and (bottom) q of MgO periclase from (bold solid lines) third order Eulerian finite strain theory (Eqns. 14,17-19), first principles calculations at 1000 K (circles) (Karki et al. 2000b) and (squares) (Oganov and Dorogokupets 2003), *ab initio* ionic models (diamonds) (Agnon and Bukowinski 1990), (up-triangles) (Inbar and Cohen 1995), an experimental analysis of the Hugoniot (double-dotted line) (Speziale et al. 2001), a combination of theory and experiment (down-triangles) (Anderson et al. 1993) and (thin solid lines) the approximation that $q = q_0$ is constant. For periclase we used V_0 = 77.24 Å^3 per unit cell to generate these plots (Karki et al. 2000b). The Eulerian finite strain results are calculated assuming the following values taken from the first principles calculations for the purposes of this comparison: γ_0 = 1.60, q_0 = 1.3 for periclase (Karki et al. 2000b). The two first principles calculations disagree in the value of γ_0 but show the same functional form. (Modified from Stixrude and Lithgow-Bertelloni 2005b).

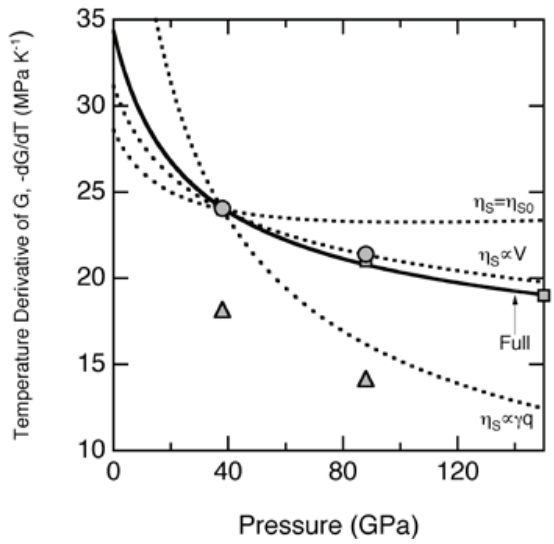

Figure 4. Temperature derivative of the shear modulus of $MgSiO_3$ perovskite from third order Eulerian finite strain theory (bold solid line) compared with density functional theory (squares, 2000-3000 K) (Wentzcovitch et al. 2004), (circles, 1500-3500 K) (Oganov et al. 2001b), an *ab initio* ionic model (PIB-Potential Induced Breathing; triangles) (Marton and Cohen, 2002) and (dashed lines) different approximations to the volume dependence of η_S: η_S arbitrarily assumed to be constant ($\eta_S = \eta_{S0}$), proportional to the volume, V, or proportional to $\eta_V = \gamma q$. The value of η_{S0} for each curve is set so that it passes through the first principles point at 38 GPa. (Modified from Stixrude and Lithgow-Bertelloni 2005b).

to capture the volume dependence predicted by density functional theory (Fig. 4). Accurate values of this parameter are critical in making comparisons between mineralogical models and seismological models as the shear wave velocity and its lateral variations in the mantle are well constrained and because the shear wave velocity is more sensitive than the longitudinal wave velocity to variations in temperature and bulk composition.

SCALING

How can we relate the physical properties of the heterogeneous, multi-phase mantle to those of laboratory scale samples, or to those of notional perfect crystals as probed with first

principles theory? There are two important issues when considering physical properties of the mantle as revealed by seismology: scaling in space and in time.

For perfect, homogeneous crystals, scaling from laboratory length scales to geophysical length scales is essentially exact (Stixrude and Jeanloz 2007). Typical grain sizes in the laboratory and in the mantle far exceed the interatomic spacing, so that dispersion of the acoustic modes away from the Brillouin zone center is negligible, even for grains as small as one micron. In first principles calculations, it is straightforward to compute the elastic wave velocities in the geophysically relevant limit, i.e., in the limit $k \to 0$, where k is a reciprocal space vector. This unity of length scales is modified by heterogeneity: e.g., the contrast in elastic properties between neighboring grains, and anelasticity (dissipation) in real rocks.

A seismic wave passing through any part of the mantle senses the elastic response of a heterogeneous composite consisting of many grains of differing size, shape, orientation, and elasticity. Therefore, while knowledge of the elastic properties of individual phases is necessary for determining the seismic wave velocity, it is not sufficient. In principle, we must also specify the geometry and elasticity of each grain; of order 10^{21} grains sampled by a typical seismic wavelength of 50 km. It is not possible, nor useful to specify the grain geometry in such detail. Instead, one may place rigorous bounds on the elastic properties of the composite from knowledge of the elastic properties of the constituents.

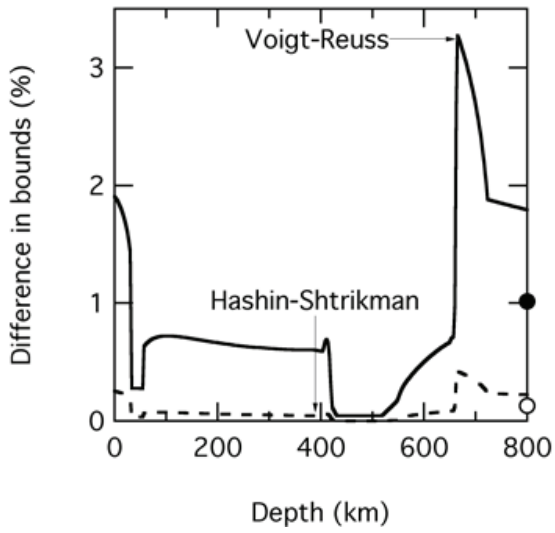

Figure 5. Computed differences between the Voigt and Reuss (solid) and Hashin-Shtrikman (dashed) bounds for S-wave velocity in a model mantle composition (Workman and Hart 2005) along a self-consistent 1600 K isentrope. Symbols represent the values at the core-mantle boundary (2891 km depth). (Modified from Stixrude and Jeanloz 2007).

The approaches of Hashin-Shtrikam (Hashin and Shtrikman 1963) and Voigt-Reuss-Hill (Hill 1963) place bounds on the effective elastic moduli of a heterogeneous aggregate (Fig. 5). The bounds depend only on properties that are determined by equilibrium thermodynamics: the elastic moduli and volume fractions of the constituent phases. The Hashin-Shtrikman bounds are rigorous under the assumption that the constituent phases are distributed randomly. The Voigt-Reuss bounds correspond, respectively to conditions of uniform strain and uniform stress across the constituent grains. Neither of these two limits is physically realizable, except in special geometries, since uniform strain violates mechanical equilibrium, and uniform stress entails grain-grain gaps and overlap. An advantage of the Voigt-Reuss bounds are that they encompass special arrangements of phases, such as layering (shape-preferred orientation), that are often encountered in the Earth (Backus 1962)

$$M^*_{\mathrm{R}} = \left(\sum_{\alpha} \frac{\phi^{\alpha}}{M^{\alpha}} \right)^{-1} < M^* < \sum_{\alpha} \phi^{\alpha} M^{\alpha} = M^*_{\mathrm{V}} \tag{20}$$

where ϕ^{α} and M^{α} are the volume fraction and elastic modulus of phase α, and asterisks indicate effective moduli, and subscripts R and V indicate, respectively Reuss and Voigt bounds. The so-called Voigt-Reuss-Hill average is the simple average of the Voigt and Reuss bounds and is not theoretically justified as a best estimate of the effective elastic moduli. Empirically, one finds for many aggregates, including those typical of the mantle that the Voigt-Reuss-Hill average

falls within the narrower Hashin-Shtrikman bounds (Watt et al. 1976). In Earth's mantle, the bounds are in any case not wide, and seldom exceed experimental uncertainty.

Seismic wave velocities depend on time scale because elastic wave propagation is dissipative in the seismic band (Anderson and Given 1982). The importance of dissipative processes such as defect migration and grain-boundary sliding are measured by the quality factor, Q defined in terms of the energy loss per cycle

$$Q^{-1} = \frac{dE}{E} \tag{21}$$

Dissipation has two important consequences, both of which can be measured seismologically: attenuation and dispersion, which refers to the dependence of the elastic wave velocity on frequency or wavelength. Experimental and seismological observations are consistent with a simple model in which attenuation is assumed to depend slightly on frequency over a broad range of frequencies (the absorption band), reflecting the wide range of dissipative mechanisms present in real materials (Anderson and Given 1982). In the limit of small dissipation, the velocity is (Jackson et al. 2002)

$$V\left(P,T,\omega\right) = V\left(P,T,\infty\right)\left[1 - \frac{1}{2}\cot\left(\frac{\alpha\pi}{2}\right)Q^{-1}\left(P,T,\omega\right)\right] \tag{22}$$

where V is the velocity, ω is the frequency, and α is an empirically determined parameter that describes the frequency dependence of Q with $\alpha = 0.26$ a typical experimental value. Because first principles theory and experiment (MHz-GHz) determine elastic properties in the infinite frequency limit, a correction for dispersion must be applied before they may be compared with seismologically determined velocities. For values of Q similar to the lowest found in one-dimensional seismological models (~80) (Romanowicz 1995), the velocity at seismic frequencies is ~1% lower than that in the infinite frequency limit.

APPLICATIONS

Origin of the low velocity zone

The origin of the low velocity zone remains enigmatic, even though this region is seismologically well established and geodynamically important (Gutenberg 1959). The low velocity zone is a region of the upper mantle in which velocity decreases with increasing depth, and is associated with a zone of reduced viscosity (asthenosphere) that may be an essential enabler of plate tectonics (Richards et al. 2001). The presence of low velocity zones in Earth-like planets is an inevitable consequence of a thermal boundary layer: the geothermal gradient is so steep that the influence of temperature on the velocity exceeds that of pressure (Stixrude 2007). The key question regarding the low velocity zone of Earth's mantle is quantitative: are the velocities so low as to require partial melt to explain them? The answer can only come from comparison to the predictions of mineralogical models of known thermodynamic state.

We have found that partial melt is not required to explain the low velocity zone, and that variations of temperature along plausible geotherms in sub-solidus mantle assemblages are sufficient to explain the seismological observations within uncertainty (Stixrude and Lithgow-Bertelloni 2005a) (Fig. 6). Our mineralogical models predict variations in the depth extent and slowness of the low velocity zone with lithospheric age that are seen seismologically. Moreover, the lowest velocities predicted are consistent with a range of seismological models of the same lithospheric age. The only part of the low velocity zone that probably requires partial melt is in the immediate vicinity of the ridge (age <5 Ma). Our conclusions differ from previous analyses based on non-self-consistent thermodynamic models in which the seismic wave velocity was assumed to vary linearly with temperature from room temperature to mantle

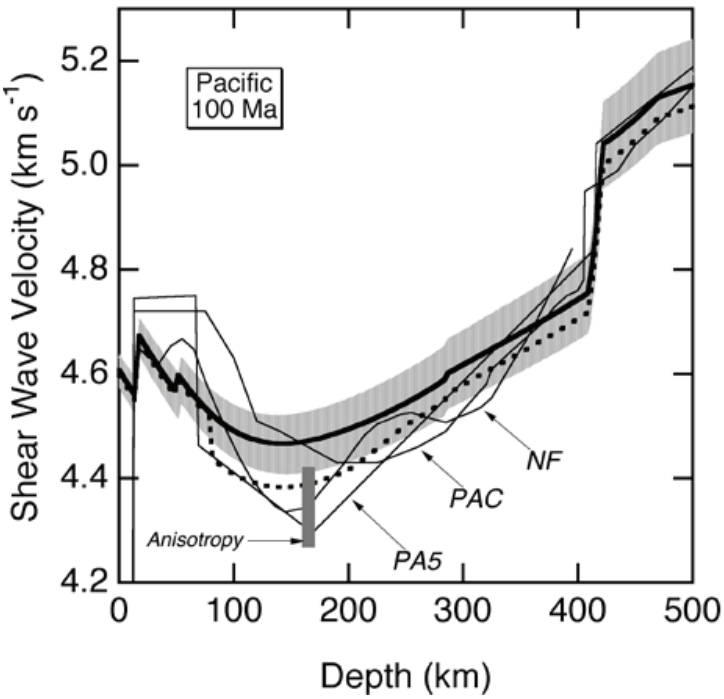

Figure 6. The shear wave velocity of pyrolite along a 100 Ma conductive cooling geotherm in the elastic limit (bold line), and including the effects of dispersion according to the seismological attenuation model QR19 (Romanowicz 1998) (bold dashed). The shading represents the uncertainty in the calculated velocity. The mineralogical model is compared with seismological models (light lines) PAC (Graves and Helmberger 1988), NF110+ (Nishimura and Forsyth 1989), and PA5 (Gaherty et al. 1999). The approximate magnitude of SH-SV anisotropy in the mantle is indicated by the vertical bar. [Used by permission of American Geophysical Union from Stixrude and Lithgow-Bertelloni (2005).]

temperatures (Birch 1969; Schubert et al. 1976). In fact, the velocity varies non-linearly with temperature particularly at temperature near room temperature and below as required by the third law, and a realistic account of the physics predicts much lower solid-phase velocities at mantle conditions.

Our study highlighted two important questions (Stixrude and Lithgow-Bertelloni 2005a). First, while our models are consistent with seismology to within mutual uncertainty, there appears to be a systematic tendency for seismological models to predict slower minimum velocities. We found that the origin of this small remaining discrepancy is unclear, but that it might be explained by small super-adiabatic variations in temperature, or inhomogeneities in composition. Second, the variation of velocity with depth deeper than the low velocity zone is much greater in seismological models. We speculated that this may be due to sub-adiabatic temperature gradients, or an increase with depth of a silica-rich component. Indeed, one recent study, which also used our thermodynamic model, showed that an increase with depth of a basaltic component could explain the high gradient zone (Cammarano et al. 2009). However, the amount of basalt enrichment required over a relatively narrow depth interval (from 5% at 250 km to 35% at 400 km) may be unrealistic, and the question of the origin of the high gradient zone remains open.

Origins of lateral heterogeneity

Seismic tomography reveals lateral variations in the elastic structure of the mantle that can often be correlated with known tectonic features at the surface (Romanowicz 2008). Many features are plausibly linked to lateral variations in temperature such as those thought to be associated with subducting slabs. Tomography holds out the promise of mapping mantle convection in the present-day Earth. Yet quantifying the origins of lateral variations in velocity

remains difficult. One of the reasons is that lateral variations in temperature alone cannot account for all of the observed structure. Lateral variations in the shear wave velocity V_S that far exceed those in the longitudinal wave velocity V_P (Bolton and Masters 2001), regions in which lateral variations in V_S and the bulk sound velocity V_B are anti-correlated (Ishii and Tromp 1999), and anomalies with sharp boundaries (Ni et al. 2002), all point to a non-thermal origin of a significant part of the mantle's three-dimensional structure.

Understanding the three-dimensional structure of the mantle requires the unraveling of three possible origins of lateral heterogeneity in Earth's mantle: lateral variations in temperature, bulk composition, and phase. Each of these contributions may have similar magnitudes. Lateral variations in bulk composition have also received considerable attention, although the origin of such lateral variations remains obscure (Trampert et al. 2004).

We have shown that lateral variations in phase assemblage have an influence on three-dimensional mantle structure comparable to lateral variations in temperature over the upper 800 km of the mantle (Stixrude and Lithgow-Bertelloni 2007). This part of Earth is replete with phase transformations, all of which have finite Clapeyron slopes, and most of which occur over a depth interval that is a substantial fraction of the wavelength of seismic probes. Phase transitions are likely to be important in explaining lateral heterogeneity near the core-mantle boundary as well (Hirose 2006).

At any depth, the mantle is made of several different phases, with distinct elastic properties. As temperature varies, the relative proportions, and compositions of these phases change, contributing to laterally varying structure. In a multi-phase assemblage, the variation with temperature of any property X, such as velocity or density, at constant pressure has two contributions

$$\left(\frac{\partial \ln X}{\partial T}\right)_P = \left(\frac{\partial \ln X}{\partial T}\right)_{P,\vec{n}} + \left(\frac{\partial \ln X}{\partial \vec{n}}\right)_{P,T}\left(\frac{\partial \vec{n}}{\partial T}\right)_P \tag{21}$$

where $\vec{n}$ is the vector specifying the amounts of all end-member species of all phases. The first term on the right hand side may be called the isomorphic part: the derivative is taken at constant amounts and compositions of all coexisting phases. The second term may be called the metamorphic part and accounts for the variations in phase proportions (and compositions) with temperature. The magnitude of the metamorphic contribution

$$\left(\frac{\partial \ln X}{\partial \vec{n}}\right)_{P,T}\left(\frac{\partial \vec{n}}{\partial T}\right)_P \approx f\Gamma\frac{\Delta \ln X}{\Delta P} \tag{22}$$

where f is the volume fraction of the mantle composed of the transforming phases, $\Delta \ln X$ is the relative difference in the property X between the two transforming phases, ΔP is the pressure range over which the transition occurs, and Γ is the effective Clapeyron slope. The effect is largest for sharp transitions, such as the olivine to wadsleyite transition, and in this case may also be described in terms of the topography of the transition. It is sensible to describe lateral variations in velocity due to phase equilibria in terms of topography when the topography exceeds the width of the phase transformation

$$\left(\frac{\partial P}{\partial T}\right)_{eq}\delta T > \Delta P \tag{23}$$

where δT is the anticipated magnitude of lateral temperature variations. The influence of phase transformations is also important for broad transitions such as pyroxene to garnet. In the upper mantle, most phase transitions have positive Clapeyron slopes. This means that, except in the vicinity of the 660 km discontinuity, phase transitions systematically increase the temperature dependence of seismic wave velocities throughout the upper 800 km of the mantle.

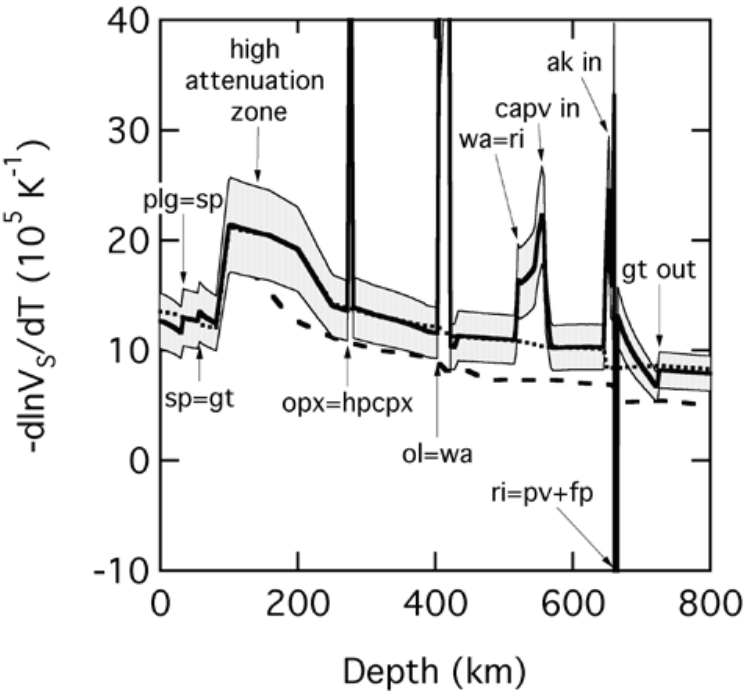

Figure 7. Temperature derivative of the shear wave velocity along the 1600 K isentrope (bold solid) and the isomorphic contribution (short dashed). The shading indicates nominal uncertainties. We compare with the results of (Cammarano et al. 2003) (long dashed). The locations of the high attenuation zone and various phase transitions are indicated with abbreviations defined in Figure 1. [Used by permission of Elsevier from Stixrude and Lithgow-Bertelloni (2007).]

The influence of phase transformations is illustrated by the temperature derivative of the shear wave velocity (Fig. 7). The derivative is positive throughout the upper 660 km of the mantle and of greater magnitude than many previous studies that neglected the influence of phase transformations. The value of the scaling varies rapidly with depth and undergoes large excursions in the vicinity of phase transformations. Several phase transformations, in addition to those responsible for the 410 and 660 km discontinuities exhibit a substantial signal. At the latter transformation, the metamorphic contribution is large and negative, reflecting the negative sign of the Clapeyron slope (Eqn. 22).

The metamorphic contribution to the thermal expansivity has an important influence on mantle dynamics that has been recognized for some time (Christensen 1995). In models of mantle convection, this contribution is often approximated only by the ringwoodite=per ovskite+ferropericlase transition. In contrast, we find that there are important metamorphic contributions over much of the upper 800 km of the mantle (Fig. 8). We illustrate by computing the complete thermal expansivity and also the mean value of the thermal expansivity over a finite temperature interval (δT). The latter quantity shows the anticipated features: the magnitude of the peaks associated with phase transformations is reduced in amplitude ($\Delta \ln \rho / \delta T$) as compared with the local temperature derivative, and spread over a broader depth interval ($\sim \Gamma \delta T$). The metamorphic term may influence dynamics near the core-mantle boundary as well (Nakagawa and Tackley 2006). A more realistic account of the thermal expansivity of multi-phase assemblages should be included in mantle flow codes (Nakagawa et al. 2009).

Our analysis highlights one of the challenges in interpreting seismic tomographic models in terms of temperature anomalies. The magnitude and even sign of the metamorphic contribution varies rapidly with depth, and much more rapidly than the typical depth-resolution of seismic tomography. This means that seismological observations (travel times and normal mode frequencies) are not sensitive to all the depth variations in $d \ln V_S / dT$ that we predict

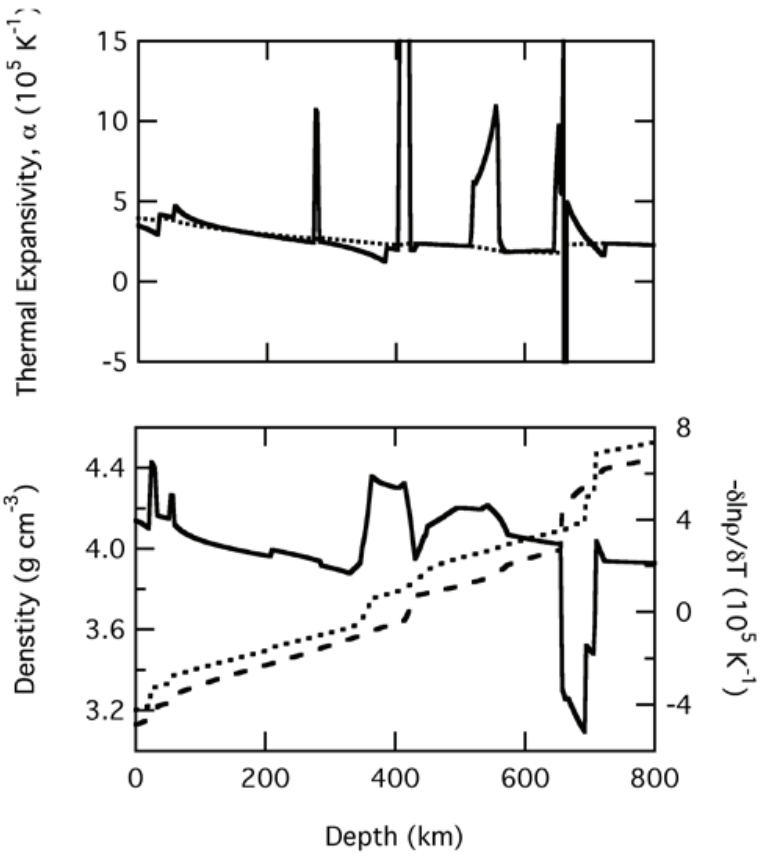

Figure 8. (top) Thermal expansivity along the 1600 K isentrope (solid) and the isomorphic contribution (dashed). (bottom) Density along 1600 K (long dashed) and 1000 K (short dashed) isentropes, and the relative difference $\delta\ln\rho/\delta T$ (solid, right-hand axis). [Used by permission of Elsevier from Stixrude and Lithgow-Bertelloni (2007).]

should exist in the mantle. Indeed, tomographic models generally find a smooth variation of the magnitude of heterogeneity with depth (Romanowicz 2003). A naïve interpretation of tomographic models, by simply scaling the observed heterogeneity to temperature using the full thermodynamically computed $d\ln V_S/dT$, produces unphysical variations with depth of the temperature heterogeneity. This problem can be overcome by inverting seismological observables directly for three-dimensional variations in temperature using our mineralogical model (Cammarano and Romanowicz 2007).

Influence of lithologic heterogeneity

Partial melting is a powerful agent of chemical differentiation that has existed throughout much of Earth's history. Most melting today occurs at mid-ocean ridges where the mantle is differentiated into a silica-rich, basaltic crust and a silica-depleted, harzburgitic layer. This differentiated package is returned to the mantle at subduction zones.

An analysis of the mass balance and diffusion rates suggests that the mantle may be composed entirely of differentiated material (Xu et al. 2008). Geochemical tracers indicate that most or all of the mantle has been differentiated at least once at a mid-ocean ridge. Moreover, the subducted differentiated material is unlikely to re-equilibrate over geologic time as the rates of chemical diffusion are so slow.

Based on this analysis, we have proposed an alternative model of the composition of the mantle (Xu et al. 2008). We view the mantle as a mechanical mixture of basalt and harzburgite. A basalt fraction of 18% produces an overall bulk composition equal to that of the MORB source and is consistent with our knowledge of subduction rates and the thickness of the oceanic crust. This picture differs considerably from the usual notion that the mantle is to first order chemically homogeneous and pyrolitic. In reality some re-equilibration between the subducted basalt and harzburgite must occur, possibly aided by fluids. In the limit of complete re-equilibration, the

mechanical mixture would revert to pyrolite. We may therefore view lithologic heterogeneity in the mantle in terms of two end-members: the mechanically mixed (MM) mantle in which no re-equilibration occurs, and the equilibrium assemblage (EA) in which lithologic heterogeneity is erased immediately upon subduction.

We have found that the mechanically mixed mantle has significantly different elastic properties from the equilibrium assemblage (Fig. 9). The reason is that the phase equilibria in the mechanical mixture are different. For example, while free silica is stable in basaltic compositions, it is not stable in pyrolite. Schematically, the phase relations may be viewed as

$$2MgSiO_3\ (EA) = Mg_2SiO_4\ (MM;\ harzburgite) + SiO_2\ (MM;\ basalt) \quad (24)$$

so that the pyroxene component in the equilibrium assemblage dissociates into olivine in the harzburgite and free silica in the basalt.

The seismic wave velocities in the mechanical mixture agree better with seismological models as compared with the equilibrium assemblage (Fig. 9). In MM, the velocity is faster and the variation of velocity with depth is greater in the transition zone. In MM, the velocity gradient is steeper also in the high gradient zone between the low velocity zone and the 410, also leading to better agreement with seismology. Both MM and EA are substantially slower along a 1600 K isentrope than the lower mantle. The origin of this discrepancy is unclear, but may be related to deviations from isentropy in the lower mantle or radial variations in bulk composition.

The mechanically mixed model of the mantle gives one a natural way of thinking about large-scale chemical heterogeneity and a plausible means of producing it (Fig. 10). In principle, describing chemical heterogeneity in the mantle is a daunting task because there are at least 6 important oxide components. But not all variations in chemical composition are geologically plausible. The mechanical mixture focuses on a type of heterogeneity that is produced by a

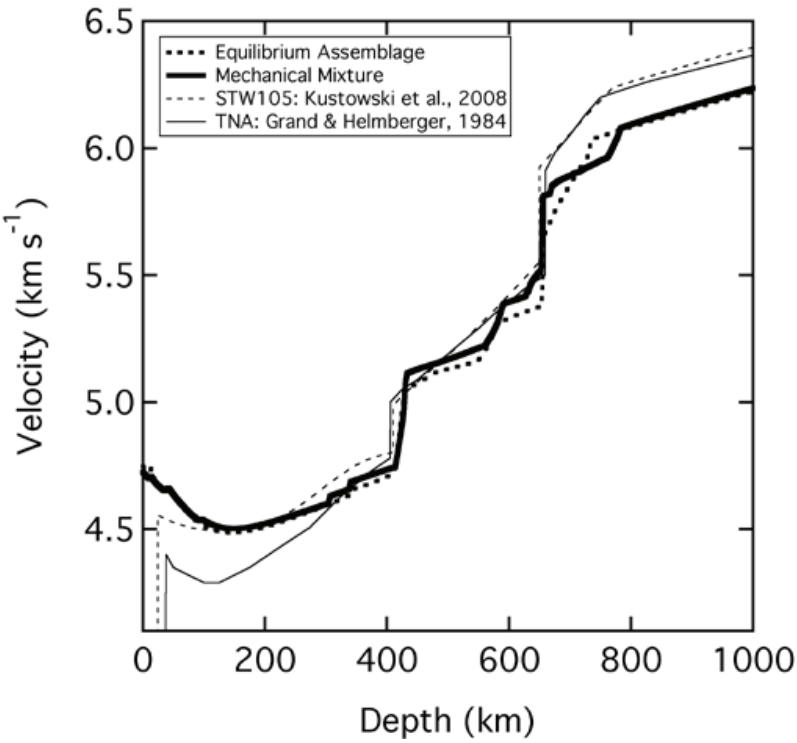

Figure 9. Shear wave velocity computed using our thermodynamic model (Xu et al. 2008) along a 1600 K isentrope modified by a half-space cooling upper thermal boundary layer (100 Ma) for (bold solid) the mechanical mixture (MM) and (bold dashed) the equilibrium assemblage (EA) compared with (thin dashed) global (Kustowski et al. 2008) and (thin solid) regional (Grand and Helmberger 1984) seismological models.

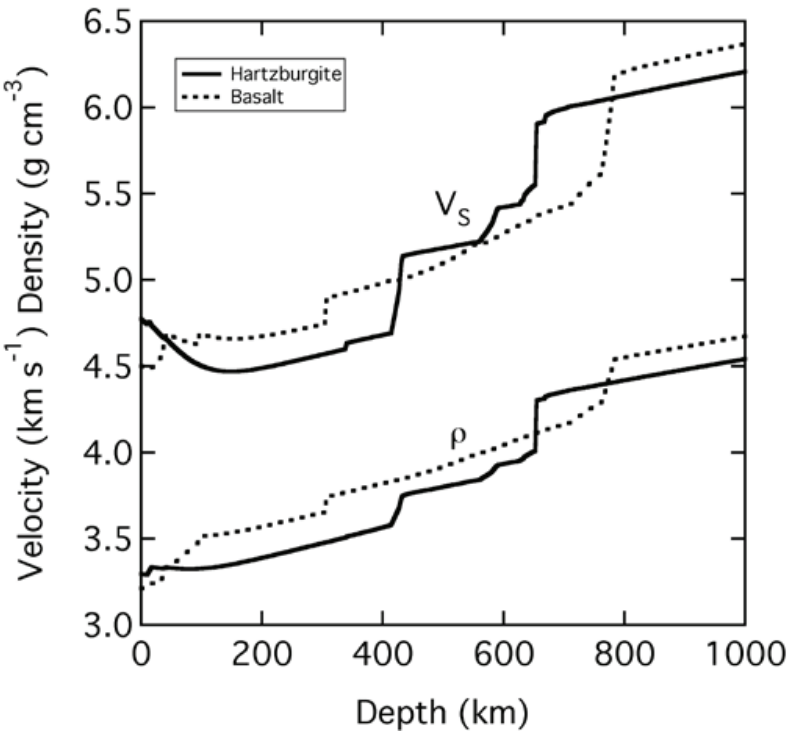

Figure 10. Shear wave velocity (V_S) and density (ρ) of basalt (dashed) and harzburgite (solid) computed using our thermodynamic model (Xu et al. 2008) along a 1600 K isentrope modified by a half-space cooling upper thermal boundary layer (100 Ma).

well-understood process (mid-ocean ridge melting) and that must be returned to the mantle. Moreover, the physical properties of the two components of the mechanical mixture are sufficiently different that they may separate dynamically and that variations in the basalt fraction should be visible seismologically throughout much of the mantle.

CONCLUSIONS AND OUTLOOK

The thermodynamic theory of Earth's mantle has developed sufficiently so that it is now possible to account self-consistently for all aspects of equilibrium that contribute to the generation of Earth structure and dynamics. The theory appears to be applicable to the entire range of sub-solidus conditions encountered in Earth's mantle. These developments have been informed by first principles theory, especially in the design and testing of functional relationships. Density functional theory has also provided predictions of key material properties that have not yet been measured experimentally.

Future challenges include expanding the scope of the thermodynamic theory to include other important classes of phases such as silicate melts (de Koker and Stixrude 2009) and metallic systems relevant to the core, and physical behavior (magnetic collapse, and electronic transitions), which will permit exploration of other regions of the mantle including the lower mantle, and other geological processes, including melt generation and differentiation, that have played a major role in Earth's history.

REFERENCES

Agnon A, Bukowinski MST (1990) Thermodynamic and elastic properties of a many-body model for simple oxides. Phys Rev B 41(11):7755-7766

Alberty RA (2001) Use of Legendre transforms in chemical thermodynamics - (IUPAC Technical Report). Pure Appl Chem 73(8):1349-1380
Allegre CJ, Turcotte DL (1986) Implications of a 2-component marble-cake mantle. Nature 323(6084):123-127
Anderson DL, Given JW (1982) Absorption-band Q model for the earth. J Geophys Res 87(NB5):3893-3904
Anderson OL, Oda H, Chopelas A, Isaak DG (1993) A thermodynamic theory of the Grüneisen ratio at extreme conditions: MgO as an example. Phys Chem Miner 19:369-380
Anderson OL, Schreiber E, Lieberman RC (1968) Some elastic constant data on minerals relevant to geophysics. Rev Geophys 6(4):491-524
Backus GE (1962) Long-wave elastic anisotropy produced by horizontal layering. J Geophys Res 67(11):4427-4400
Berman RG (1988) Internally-consistent thermodynamic data for minerals in the system Na_2O-K_2O-CaO-MgO-FeO-Fe_2O_3-Al_2O_3-SiO_2-TiO_2-H_2O-CO_2. J Petrol 29(2):445-522
Birch F (1969) Density and compostion of the upper mantle: first approximation as an olivine layer. *In*: The Earth's Crust and Upper Mantle. Hart PJ (ed) American Geophysical Union, Washington, DC, p. 18-36
Birch F (1978) Finite strain isotherm and velocities for single-crystal and polycrystalline NaCl at high-pressure and 300-degree-K. J Geophys Res 83:1257-1268
Bolton H, Masters G (2001) Travel times of P and S from the global digital seismic networks: Implications for the relative variation of P and S velocity in the mantle. J Geophys Res-Solid Earth 106(B7):13527-13540
Boyd FR (1989) Compositional distinction between oceanic and cratonic lithosphere. Earth Planet Sci Lett 96(1-2):15-26
Callen HB (1960) Thermodynamics. John Wiley and Sons, New York
Cammarano F, Goes S, Vacher P, Giardini D (2003) Inferring upper-mantle temperatures from seismic velocities. Phys Earth Planet Inter 138(3-4):197-222
Cammarano F, Romanowicz B (2007) Insights into the nature of the transition zone from physically constrained inversion of long-period seismic data. Proc Nat Acad Sci USA 104(22):9139-9144
Cammarano F, Romanowicz B, Stixrude L, Lithgow-Bertelloni C, Xu WB (2009) Inferring the thermochemical structure of the upper mantle from seismic data. Geophys J Int 179(2):1169-1185
Canup RM (2004) Dynamics of lunar formation. Ann Rev Astron Astrophys 42:441-475
Christensen U (1995) Effects of phase transitions on mantle convection. Ann Rev Earth Planet Sci 23:65-87
Cococcioni M (2010) Accurate and efficient calculations on strongly correlated minerals with the LDA+U method: review and perspectives. Rev Mineral Geochem 71:147-167
Collerson KD, Hapugoda S, Kamber BS, Williams Q (2000) Rocks from the mantle transition zone: Majorite-bearing xenoliths from Malaita, southwest Pacific. Science 288(5469):1215-1223
Davies GF (1974) Effective elastic-moduli under hydrostatic stress .1. Quasi-harmonic theory. J Phys Chem Solids 35(11):1513-1520
de Koker NP, Stixrude L (2009) Self-consistent thermodynamic description of silicate liquids, with application to shock melting of MgO periclase and $MgSiO_3$ perovskite. Geophys J Int 178:162-179
Dziewonski AM, Anderson DL (1981) Preliminary reference earth model. Phys Earth Planet Inter 25:297-356
Fei YW, Saxena SK (1990) Internally consistent thermodynamic data and equilibrium phase-relations for compounds in the system MgO-SiO_2 at high-pressure and high-pressure and high-temperature. J Geophys Res-Solid Earth Planets 95(B5):6915-6928
Gaherty JB, Kato M, Jordan TH (1999) Seismological structure of the upper mantle: a regional comparison of seismic layering. Phys Earth Planet Inter 110(1-2):21-41
Ghiorso MS, Sack RO (1995) Chemical mass-transfer in magmatic processes. 4. A revised and internally consistent thermodynamic model for the interpolation and extrapolation of liquid-solid equilibria in magmatic systems at elevated-temperatures and pressures. Contrib Mineral Petrol 119(2-3):197-212
Gramsch SA, Cohen RE, Savrasov SY (2003) Structure, metal-insulator transitions, and magnetic properties of FeO at high pressures. Am Mineral 88(2-3):257-261
Grand SP, Helmberger DV (1984) Upper mantle shear structure of North-America. Geophys J Royal Astron Soc 76(2):399-438
Graves RW, Helmberger DV (1988) Upper mantle cross-section from Tonga to Newfoundland. J Geophys Res-Solid Earth and Planets 93(B5):4701-4711
Gutenberg B (1959) Physics of the Earth's Interior. Academic Press, New York
Hacker BR, Abers GA, Peacock SM (2003) Subduction factory - 1. Theoretical mineralogy, densities, seismic wave speeds, and H_2O contents. J Geophys Res-Solid Earth 108(B1):2029, doi: 10.1029/2001JB001127
Hama J, Suito K (1998) High-temperature equation of state of $CaSiO_3$ perovskite and its implications for the lower mantle. Phys Earth Planet Inter 105(1-2):33-46
Hashin Z, Shtrikman S (1963) A variational approach to the theory of the elastic behaviour of multiphase materials. J Mech Phys Solids 11(2):127-140
Hill R (1963) Elastic properties of reinforced solids - some theoretical principles. J Mech Phys Solids 11(5):357-372

Hirose K (2006) Postperovskite phase transition and its geophysical implications. Rev Geophys 44(3):Art. No. RG3001, doi: 10.1029/2005RG000186

Hirschmann MM (2006) Water, melting, and the deep Earth H_2O cycle. Ann Rev Earth Planet Sci 34:629-653

Holland TJB, Powell R (1998) An internally consistent thermodynamic data set for phases of petrological interest. J Metamorph Geol 16(3):309-343

Inbar I, Cohen RE (1995) High pressure effects on thermal properties of MgO. Geophys Res Lett 22:1533-1536

Isaak DG, Anderson OL, Cohen RE (1992) The relationship between shear and compressional velocities at high pressures: reconciliation of seismic tomography and mineral physics. Geophys Res Lett 19:741-744

Ishii M, Tromp J (1999) Normal-mode and free-air gravity constraints on lateral variations in velocity and density of Earth's mantle. Science 285(5431):1231-1236

Ita J, Stixrude L (1992) Petrology, elasticity, and composition of the mantle transition zone. J Geophys Res-Solid Earth 97(B5):6849-6866

Jackson I, Gerald JDF, Faul UH, Tan BH (2002) Grain-size-sensitive seismic wave attenuation in polycrystalline olivine. J Geophys Res-Solid Earth 107(B12):2360

Karki BB, Stixrude L, Clark SJ, Warren MC, Ackland GJ, Crain J (1997) Elastic properties of orthorhombic $MgSiO_3$ perovskite at lower mantle pressures. Am Mineral 82:635-638

Karki BB, Wentzcovitch RM, de Gironcoli S, Baroni S (2000a) Ab initio lattice dynamics of $MgSiO_3$ perovskite at high pressure. Phys Rev B 62(22):14750-14756

Karki BB, Wentzcovitch RM, de Gironcoli S, Baroni S (2000b) High-pressure lattice dynamics and thermoelasticity of MgO. Phys Rev B 61(13):8793-8800

Kohn W (1999) Nobel lecture: electronic structure of matter-wave functions and density functionals. Rev Mod Phys 71(5):1253-1266

Kuskov OL (1995) Constitution of the Moon. 3. Composition of middle mantle from seismic data. Phys Earth Planet Inter 90(1-2):55-74

Kustowski B, Ekstrom G, Dziewonski AM (2008) Anisotropic shear-wave velocity structure of the Earth's mantle: A global model. J Geophys Res-Solid Earth 113(B6):B06306, doi: 10.1029/2007JB005169

Mao WL, Mao HK, Sturhahn W, Zhao JY, Prakapenka VB, Meng Y, Shu JF, Fei YW, Hemley RJ (2006) Iron-rich post-perovskite and the origin of ultralow-velocity zones. Science 312(5773):564-565

Marton FC, Cohen RE (2002) Constraints on lower mantle composition from molecular dynamics simulations of $MgSiO_3$ perovskite. Phys Earth Planet Inter 134(3-4):239-252

Mattern E, Matas J, Ricard Y, Bass J (2005) Lower mantle composition and temperature from mineral physics and thermodynamic modelling. Geophys J Int 160(3):973-990

McKenzie D, Bickle MJ (1988) The volume and composition of melt generated by extension of the lithosphere. J Petrol 29(3):625-679

Mitas L, Kolorenč J (2010) Quantum Monte Carlo studies of transition metal oxides. Rev Mineral Geochem 71:137-145

Murakami M, Hirose K, Kawamura K, Sata N, Ohishi Y (2004) Post-perovskite phase transition in $MgSiO_3$. Science 304(5672):855-858

Murakami M, Sinogeikin SV, Hellwig H, Bass JD, Li J (2007) Sound velocity of $MgSiO_3$ perovskite to Mbar pressure. Earth Planet Sci Lett 256(1-2):47-54

Nakagawa T, Tackley PJ (2006) Three-dimensional structures and dynamics in the deep mantle: Effects of post-perovskite phase change and deep mantle layering. Geophys Res Lett 33(12):L12S11, doi: 10.1029/2006GL025719

Nakagawa T, Tackley PJ, Deschamps F, Connolly JAD (2009) Influence of MORB bulk composition on 3-D spherical models of thermo-chemical mantle convection with self-consistently calculated mineral physics. Geochim Cosmochim Acta 73(13):A929-A929

Ni SD, Tan E, Gurnis M, Helmberger D (2002) Sharp sides to the African superplume. Science 296(5574):1850-1852

Nishimura CE, Forsyth DW (1989) The anisotropic structure of the upper mantle in the Pacific. Geophys J Oxford 96(2):203-229

Oganov AR, Brodholt JP, Price GD (2001a) Ab initio elasticity and thermal equation of state of $MgSiO_3$ perovskite. Earth Planet Sci Lett 184:555-560

Oganov AR, Brodholt JP, Price GD (2001b) The elastic constants of $MgSiO_3$ perovskite at pressures and temperatures of the Earth's mantle. Nature 411(6840):934-937

Oganov AR, Dorogokupets PI (2003) All-electron and pseudopotential study of MgO: Equation of state, anharmonicity, and stability. Phys Rev B 67(22):224110, doi: 10.1103/PhysRevB.67.224110

Ohtani E, Sakai T (2008) Recent advances in the study of mantle phase transitions. Phys Earth Planet Inter 170(3-4):240-247

Perdew JP, Ruzsinszky A (2010) Density functional theory of electronic structure: a short course for mineralogists and geophysicists. Rev Mineral Geochem 71:1-18

Richards MA, Yang WS, Baumgardner JR, Bunge HP (2001) Role of a low-viscosity zone in stabilizing plate tectonics: Implications for comparative terrestrial planetology. Geochem Geophys Geosys 2: 2000GC000115

Romanowicz B (1995) A global tomographic model of shear attenuation in the upper-mantle. J Geophys Res-Solid Earth 100(B7):12375-12394

Romanowicz B (1998) Attenuation tomography of the earth's mantle: A review of current status. Pure Appl Geophys 153(2-4):257-272

Romanowicz B (2003) Global mantle tomography: progress status in the past 10 years. Ann Rev Earth Planet Sci 31:303-328

Romanowicz B (2008) Using seismic waves to image Earth's internal structure. Nature 451(7176):266-268

Schubert G, Froidevaux C, Yuen DA (1976) Oceanic lithosphere and asthenosphere - thermal and mechanical structure. J Geophys Res 81(20):3525-3540

Sobolev SV, Babeyko AY (1994) Modeling of mineralogical composition, density and elastic-wave velocities in anhydrous magmatic rocks. Surveys in Geophysics 15(5):515-544

Speziale S, Zha CS, Duffy TS, Hemley RJ, Mao HK (2001) Quasi-hydrostatic compression of magnesium oxide to 52 GPa: Implications for the pressure-volume-temperature equation of state. J Geophys Res-Solid Earth 106(B1):515-528

Stixrude L (2007) Properties of rocks and minerals - Seismic properties of rocks and minerals, and structure of the Earth. *In:* Mineral Physics, Vol. 2. Price GD (ed) Elsevier, Amsterdam, p 7-32

Stixrude L, Bukowinski MST (1990) Fundamental thermodynamic relations and silicate melting with implications for the constitution of D''. J Geophys Res 95:19311-19325

Stixrude L, Jeanloz R (2007) Constraints on seismic models from other disciplines - Constraints from mineral physics on seismological models. *In*: Seismology and Structure of the Earth, Vol. 1. Dziewonski AM, Romanowicz B (eds) Elsevier, Amsterdam, p. 775-803

Stixrude L, Lithgow-Bertelloni C (2005a) Mineralogy and elasticity of the oceanic upper mantle: Origin of the low-velocity zone. J Geophys Res-Solid Earth 110(B3):B03204, doi: 10.1029/2004JB002965

Stixrude L, Lithgow-Bertelloni C (2005b) Thermodynamics of mantle minerals - I. Physical properties. Geophys J Int 162(2):610-632

Stixrude L, Lithgow-Bertelloni C (2007) Influence of phase transformations on lateral heterogeneity and dynamics in Earth's mantle. Earth Planet Sci Lett 263(1-2):45-55

Thompson JB (1969) Chemical reactions in crystals. Am Mineral 54(3-4):341-375

Trampert J, Deschamps F, Resovsky J, Yuen D (2004) Probabilistic tomography maps chemical heterogeneities throughout the lower mantle. Science 306(5697):853-856

Valencia D, O'Connell RJ, Sasselov D (2006) Internal structure of massive terrestrial planets. Icarus 181(2):545-554

Wallace DC (1972) Thermodynamics of Crystals. John Wiley and Sons, New York

Watt JP, Davies GF, Connell RJO (1976) The elastic properties of composite materials. Rev Geophys Space Phys 14:541-563

Wentzcovitch RM, Karki BB, Cococcioni M, de Gironcoli S (2004) Thermoelastic properties of $MgSiO_3$-perovskite: Insights on the nature of the Earth's lower mantle. Phys Rev Lett 92(1):018501, doi: 10.1103/PhysRevLett.92.018501

Wentzcovitch RM, Yu YG, Wu Z (2010) Thermodynamic properties and phase relations in mantle minerals investigated by first principles quasiharmonic theory. Rev Mineral Geochem 71:59-98

Workman RK, Hart SR (2005) Major and trace element composition of the depleted MORB mantle (DMM). Earth Planet Sci Lett 231(1-2):53-72

Xie SX, Tackley PJ (2004) Evolution of helium and argon isotopes in a convecting mantle. Phys Earth Planet Inter 146(3-4):417-439

Xu WB, Lithgow-Bertelloni C, Stixrude L, Ritsema J (2008) The effect of bulk composition and temperature on mantle seismic structure. Earth Planet Sci Lett 275(1-2):70-79